

Synthesis and Properties of Bilirubin Analogs With Conformation-Perturbing C(10) *tert*-Butyl and Adamantyl Groups

Ari K. Kar and David A. Lightner*

Department of Chemistry, University of Nevada, Reno, Nevada 89557-0020 USA

Received 20 April 1998; revised 3 August 1998; accepted 4 August 1998

Abstract. Bilirubin analogs with *tert*-butyl (**1**) and adamantyl (**2**) substituents at the central carbon have been synthesized by reaction of an α -H dipyrinone with pivaldehyde or 1-formyladamantane. The pigments are shown by NMR to adopt an intramolecularly hydrogen-bonded ridge-tile conformation. However, unlike their parent unsubstituted rubin (**5**), the ridge-tile is distorted from C_2 symmetry by nonbonded steric interactions between the bulky C(10) substituents and the proximal propionic acid chain. © 1998 Elsevier Science Ltd. All rights reserved.

Introduction

The important and structurally interesting mammalian natural product, bilirubin (Fig. 1), is the yellow-orange pigment of jaundice and is produced copiously in normal human metabolism from turnover of hemoglobin and other heme proteins.¹⁻³ Considerable effort has been devoted to understanding the properties and metabolism of bilirubin, with particular attention being focussed on its unique ability to fold

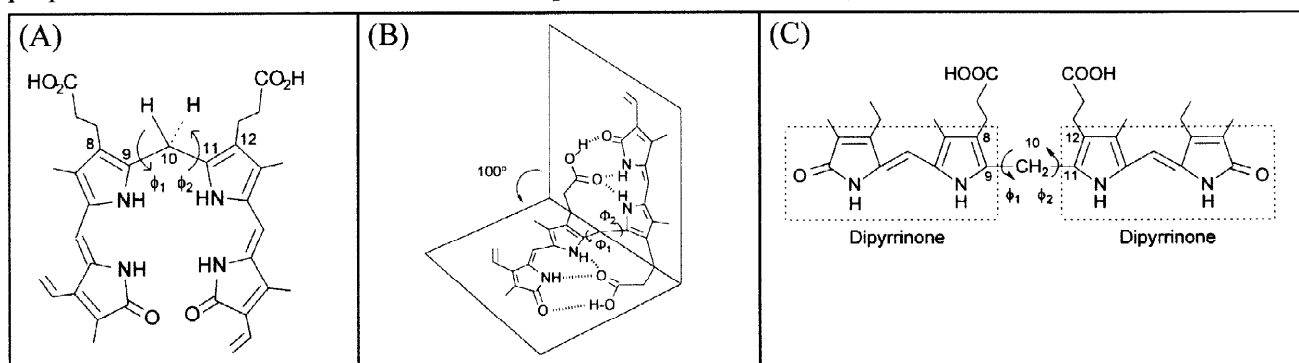


FIGURE 1. (A) Bilirubin in a high energy porphyrin-like conformation with angles of rotation about the C(9)-C(10) and C(10)-C(11) bonds, ϕ_1 and ϕ_2 , $\sim 0^\circ$. (B) Preferred bilirubin conformation shaped like a ridge-tile with $\phi_1 = \phi_2 \sim 60^\circ$ and an interplanar angle of $\sim 100^\circ$. This conformation achieves considerable stabilization from intramolecular hydrogen bonds (hatched lines). (C) Mesobilirubin-XIII α shown in a high energy, linear conformational representation. Like bilirubin, mesobilirubin has two dipyrinone chromophores, but neither pigment prefers the linear conformation. Rotations about torsion angles ϕ_1 and ϕ_2 interconvert the porphyrin-like, ridge-tile and linear conformations.

into a conformation where the carboxylic acid groups are sequestered through intramolecular hydrogen bonding (Fig. 1B).⁴⁻⁶ Such hydrogen bonding decreases the polarity of the pigment and renders it unexcretable in normal metabolism, except by glucuronidation.^{1,7} Relocation of bilirubin's propionic acid groups from the natural locations at C(8) and C(12) prevents intramolecular hydrogen bonding in more polar analogs that do not require glucuronidation for hepatic excretion.^{7,8} However, analogs with propionic acid groups at C(8) and C(12), such as the synthetic analog mesobilirubin-XIII α (Fig. 1C), typically exhibit the same unique polarity and excretable properties as bilirubin. For these pigments, like bilirubin, can tuck their carboxylic acid groups inward, where they are tethered to an opposing dipyrinone by intramolecular hydrogen bonding (Fig. 1B).

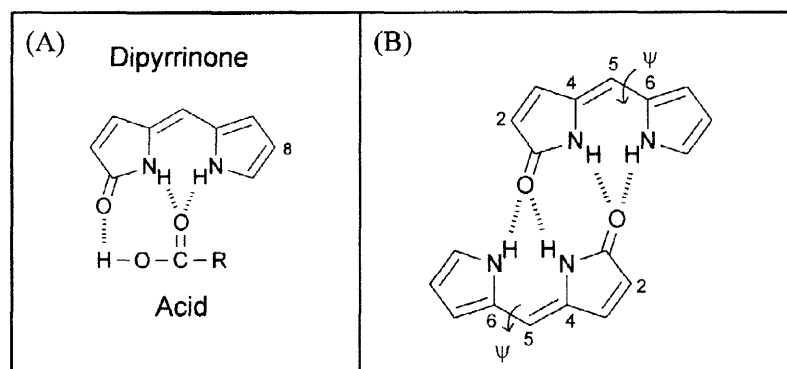
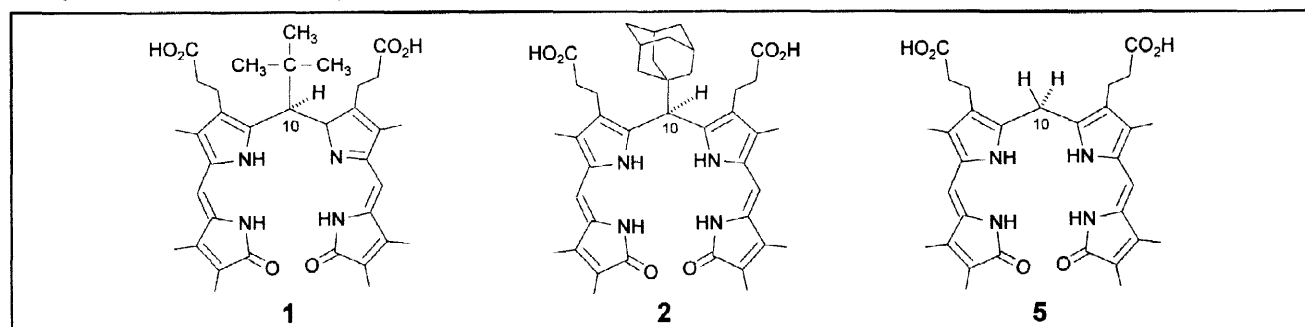


FIGURE 2. (A) Acid to dipyrinone hydrogen bonding found in bilirubin and its analogs with propionic acids at C(8) and/or C(12), and in dipyrinones with alkanolic acids at C(8). (B) Dipyrinone to dipyrinone hydrogen bonding found in bilirubin esters, rubins incapable of intramolecular hydrogen bonding and in many dipyrinones. Rotations about the C(5)-C(6) bond, torsion angle ψ , cause the dipyrinone to twist out of the planar conformation (where $\psi \sim 0^\circ$).

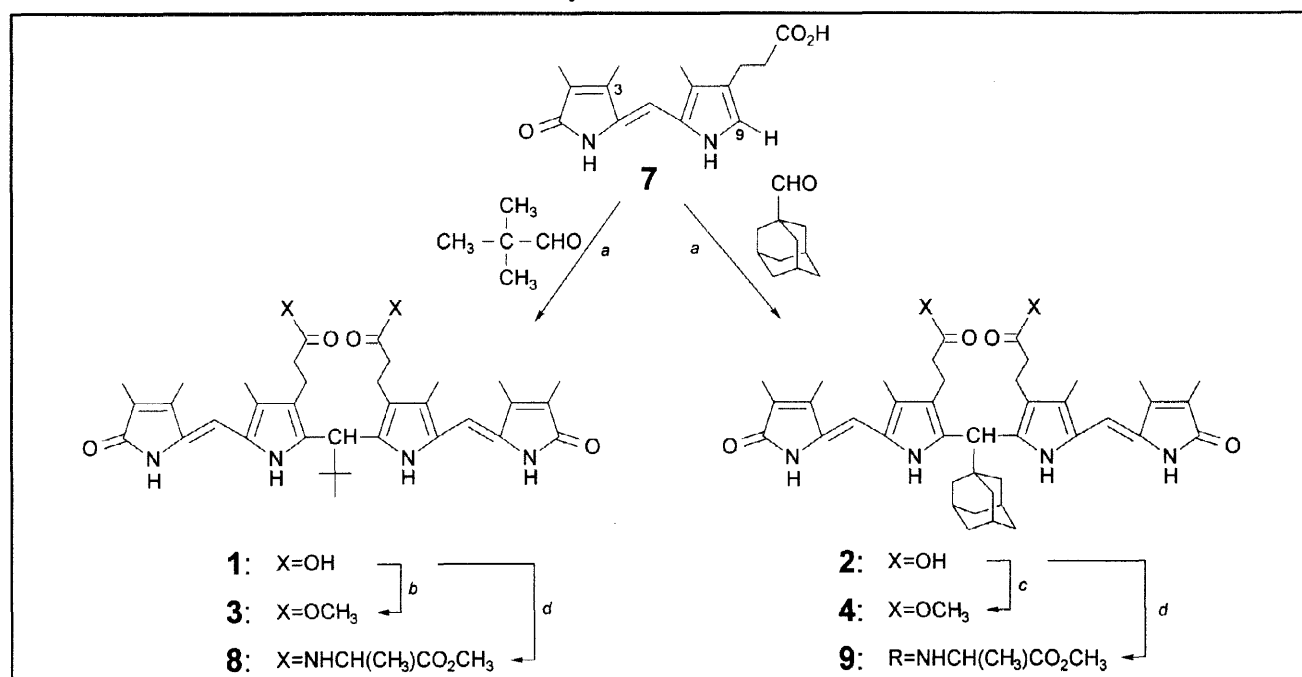
Carboxylic acid to dipyrinone hydrogen bonding, depicted in Fig. 2A is favored over dipyrinone to dipyrinone hydrogen bonding (Fig. 2B) and is one of the most interesting and important facets of bilirubin structure.⁴⁻⁸ Although the two component dipyrinone units of bilirubin and its analogs may rotate relatively freely and independently about the interconnecting C(10) CH₂ group (Fig. 1), only two conformations are uniquely stabilized through an extensive network of intramolecular hydrogen bonds: that shown in Fig. 1B and its enantiomer, which (for bilirubin and mesobilirubin) are known to interconvert fairly rapidly at room temperature over a barrier of ~ 20 kcal/mole.^{4,6,9} Our interest in bilirubin stereochemistry and its stabilization by intramolecular hydrogen bonding between propionic acid and dipyrinone groups led us to consider whether such hydrogen bonding might be retained in bilirubin analogs with bulky substituents located at C(10), i.e., at the ridge-tile seam. In the following, we report on the synthesis, properties and conformational analysis of new, symmetric analogs of rubin **5**,¹⁰ with *tert*-butyl (**1**) and 1-adamantyl (**2**) substituents at C(10). The spectral properties of **1** and **2** are correlated with stereochemical analysis from molecular dynamics simulations.



Results and discussion

Synthesis. The target bilirubins **1** and **2** were prepared in 66 and 31% yield, respectively (Synthetic Scheme) in straightforward fashion by trifluoroacetic acid-catalyzed reaction of the known 3,9-bisnor-xanthobilirubic acid (**7**) with either pivalaldehyde or 1-formyladamantane¹² in dichloromethane. The corresponding dimethyl esters (**3** and **4**) were prepared using diazomethane or cesium carbonate plus methyl iodide. Rubin acids **1** and **2** were converted to their bis-amides of *S*(+)-alanine methyl ester in ~70% yield using Shioiri's reagent.^{10b,13}

Synthetic Scheme



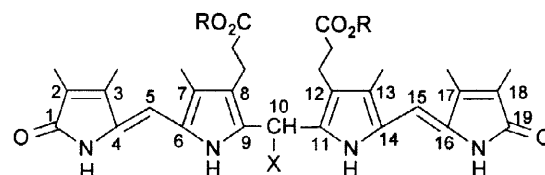
^a TFA; ^b CH₂N₂; ^c Cs₂CO₃/CH₃I/DMF; ^d L-alanine methyl ester hydrochloride / Et₃N / (C₆H₅O)₂PON₃.

Polarity from Chromatographic Behavior. Counter-intuitively, the presence of lipophilic *tert*-butyl (**1**) and adamantyl (**2**) groups at C(10) of the parent rubin analog (**5**) produces unexpectedly short retention times for **1** and rather long retention times for **2** (**1**, 13.4 min.; **2**, 26.5 min.; **5**, 14.9 min.) on reverse-phase HPLC, suggesting that **1** is more polar than **5**, and **2** is less polar. In comparison, mesobilirubin-XIII α (Fig. 1C) has a retention time of 18.3 min. Somewhat contradictorily, on silica gel TLC, **1** and **2** have much smaller R_f values (**1**, 0.55; **2**, 0.64) when compared with the parent (**5**, 0.86), which is slightly more mobile than mesobilirubin-XIII α (R_f=0.81) using 2% CH₃OH in CH₂Cl₂ as eluent. The data hint at the possibility that bulky C(10) substituents cause conformational deformations that weaken intramolecular hydrogen bonding, thereby exposing the pigment's polar groups.

¹³C-NMR and Structure. The ¹³C-NMR spectral data (Table 1) of **1** and **2** differ little, except for signals due to the C(10) substituents. Both sets of data correlate nicely with the ¹³C-NMR spectrum of the parent

rubin (**5**). Interestingly, the largest difference in chemical shift (~ 6 ppm) between **5** and **1** or **2** is at C(3)/C(17), which are remote from C(10). Certain other ring carbons remote from C(10) in **1** and **2** show a large deshieldings relative to the parent (**5**): ~ 3 ppm at C(6)/C(14), but most ring carbons of **1** and **2** show chemical shifts that are within 1-1.5 ppm of the corresponding carbons of **5**. The expected exception is the large difference (~ 4 ppm) at C(9)/C(11), which are adjacent to the substitution center. These large differences are absent or considerably reduced in the spectra of dimethyl esters **3**, **4** and **6**, suggesting different conformations for the acids and their esters.

TABLE 1. ^{13}C -NMR Chemical Shifts of Bilirubin Acids (R=H): **1** (X= *tert*-butyl), **2** (X= 1-Adamantyl), **5** (X=H) and Their Corresponding Dimethyl Esters (R=CH₃): **3**, **4** and **6**.^a

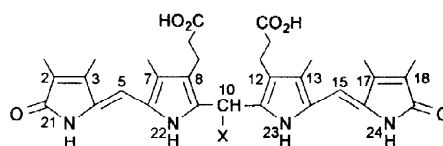


Carbon ^b Position	^{13}C Chemical Shift (δ , ppm) ^c in (CD ₃) ₂ SO					
	1	2	5	3	4	6
1,19 C=O	174.33	174.35	174.03	172.51	172.42	172.13
2,18 =C-	123.55	123.58	122.54	123.50	123.55	123.17
2 ¹ ,18 ¹ CH ₃	8.70	8.73	8.10	8.70	8.73	8.17
3,17 =C-	141.66	141.60	147.23	141.63	141.55	140.95
3 ¹ ,17 ¹ CH ₃	9.96	9.99	9.40	9.94	10.45	9.59
4,16 =C-	131.12	129.99	130.88	131.13	129.96	130.33
5,15 =CH-	99.27	99.24	97.80	99.17	99.19	97.94
6,14 =C-	125.63	125.62	122.00	125.62	125.62	123.51
7,13 =C-	120.30	121.24	122.90	120.52	120.80	122.75
7 ¹ ,13 ¹ CH ₃	10.41	10.49	9.25	10.33	9.99	9.25
8,12 =C-	120.12	120.05	119.23	120.12	120.00	118.97
8 ¹ ,12 ¹ CH ₂	20.30	20.36	19.27	20.31	20.33	19.34
8 ² ,12 ² CH ₂	35.24	35.40	34.34	34.76	34.92	34.12
8 ³ ,12 ³ C=O	172.51	172.42	172.00	173.17	173.20	173.31
8 ⁴ ,12 ⁴ OCH ₃	—	—	—	51.54	51.62	50.91
9,11 =C-	132.90	132.82	128.81	132.85	132.83	130.57
10 CH ₂ CH	43.99	45.35	23.55	44.27	45.48	23.71
10 ¹ CH ₃ C	35.82	37.56	—	35.79	37.54	—
10 ² CH ₂	29.63	41.26	—	29.58	41.16	—
10 ³ CH	—	28.63	—	—	28.58	—
10 ⁴ CH ₂	—	36.71	—	—	36.68	—

^a Run at 2.5×10^{-2} M concentration of pigment at 22°C. Multiplicities are determined by the APT method. ^b Superscripts refer to carbons in the β -substituent chains, e.g., 2¹ is the first carbon attached to ring carbon 2. ^c δ , ppm downfield from (CH₃)₄Si.

Analysis of Hydrogen Bonding and Conformation by $^1\text{H-NMR}$. Hydrogen bonding causes large deshieldings of dipyrinone lactam and pyrrole N-Hs, from ~ 7.5 and 8 ppm, respectively, in the monomer to ~ 11 and 10 ppm, respectively, in the intermolecularly hydrogen-bonded dimer in CDCl_3 (Fig. 2B).^{14,15} In bilirubins, dipyrinone N-H chemical shifts have proven to be an excellent way to assess the presence and nature of hydrogen bonding.^{10,16,17} These and other $^1\text{H-NMR}$ studies^{4,6} showed that the pyrrole N-H chemical shift is ~ 9.2 ppm in CDCl_3 (e.g., **5**, Table 2) when the dipyrinone and carboxylic acid groups are linked by intramolecular hydrogen bonding (Figs. 1B and 2A).^{10,16,17} The ~ 1 ppm shielding relative to that found in the planar dipyrinone dimer (Fig. 2B)^{14,15} may be attributed to the positioning of the pyrrole N-H to lie above the opposing pyrrole or dipyrinone π -system when the pigments adopt a ridge-tile shape (Fig. 1B). A similar but larger shielding effect is found in dipyrinone stacked dimers.¹⁵ Thus, the pyrrole N-H chemical shifts of **1**, **2** and **5** (Table 2) are consistent with acid to dipyrinone intramolecular hydrogen bonding of the type shown in Figure 1B. (The more deshielded lactam N-H and CO_2H chemical shifts in **1** and **2** as compared with the parent, **5**, suggest stronger hydrogen bonding in the analogs.)

TABLE 2. $^1\text{H-NMR}$ Chemical Shifts^a and Multiplicities for Bilirubin Analogs: **1** (X = *t*-butyl), **2** (X = 1-Adamantyl), and **5** (X = H) in CDCl_3 and $(\text{CD}_3)_2\text{SO}$.



Hydrogen ^b Position	CDCl_3			$(\text{CD}_3)_2\text{SO}$		
	1	2	5	1	2	5
$8^3, 12^3 \text{CO}_2\text{H}$	14.04	14.30 14.50	13.59	12.10	12.00	11.89
21,24 NH	11.47 10.91	11.49 10.94	10.61	9.47	9.32	9.78
22,23 NH	9.32 9.09	9.32 9.12	9.15	9.78	9.70	10.32
5,15 =CH-	6.05 6.02	6.08 6.03	6.04	6.04	5.99	5.94
10 CH ₂ CH	4.63	4.51	4.07	4.12	3.89	3.95
10^1C	—	—	—	—	—	—
$10^2 \text{CH}_3/\text{CH}_2$	1.22	2.04 (2H) 1.43 (4H)	—	1.07	1.60	—
10^3CH	—	2.03	—	—	1.95	—
10^4CH_2	—	1.69	—	—	1.60	—
$8^1, 12^1 \text{CH}_2$	3.45, ^{bcd} 3.07 ^{cef} 2.65, ^{dgh} 2.53 ^{fgh}	3.64, ^{gij} 3.08 ^{efg} 2.70, ^{ghj} 2.54 ^{fgh}	2.99 ^{kl} 2.54 ^{lm}	2.66 ⁿ	2.62 ⁿ	2.41 ⁿ
$8^2, 12^2 \text{CH}_2$	3.03, ^{bgo} 2.87 ^{egp} 2.78, ^{cho} 2.78 ^{chp}	3.04, ^{gio} 2.88 ^{egq} 2.82, ^{gho} 2.82 ^{ghq}	2.89 ^{klr} 2.78 ^{lmr}	2.20 ⁿ	2.19 ⁿ	2.05 ⁿ
$7^1, 13^1 \text{CH}_3$	2.17	2.20 2.19	2.16	2.10	2.06	2.05
$3^1, 17^1 \text{CH}_3$	2.06	2.08 2.07	2.06	2.00	1.96	2.00
$2^1, 18^1 \text{CH}_3$	1.85	1.87	1.85	1.82	1.77	1.77

^a δ , ppm downfield from $(\text{CH}_3)_4\text{Si}$ and J values in Hertz for ddd (except where noted) for 4×10^{-4} M solutions at 22°C. ^b J = 12.50. ^c J = 3.00. ^d -14.50. ^e J = 13.00. ^f J = -15.00. ^g J = 2.50. ^h J = 4.50. ⁱ J = 12.25. ^j J = -14.25. ^k J = 13.50. ^l J = 2.60. ^m J = 4.60. ⁿ t, J = 7.80. ^o J = -19.00. ^p J = -17.50. ^q J = -18.25. ^r J = -18.70 Hz.

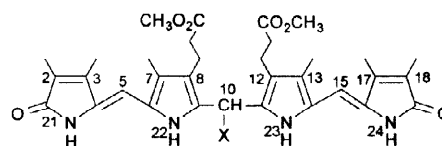
In CDCl_3 , the $^1\text{H-NMR}$ chemical shifts of the CO_2H and dipyrinone N-Hs provide strong, consistent evidence for intramolecular hydrogen bonding. Most of the $^1\text{H-NMR}$ signals of **1** and **2** are doubled (Table 1). One set of lactam N-H resonances appears ~ 0.5 ppm more deshielded than the other, which is comparable to that found in **5**. The emerging picture is one of a nonsymmetric bilirubin core folded into a ridge-tile shape (as in Fig. 1B). Nonbonded steric interactions between the bulky *tert*-butyl or adamantyl groups and the propionic acid $\alpha\text{-CH}_2$ group^{4,17} apparently squeeze one dipyrinone closer to an opposing CO_2H , thereby intensifying one hydrogen bonding triad while weakening the other and creating molecular dissymmetry.

For bilirubins in $(\text{CD}_3)_2\text{SO}$, which is thought to interpose solvent molecules into the hydrogen bonding matrix,^{6c,18} the CO_2H and lactam N-H signals become more shielded than in CDCl_3 , but the pyrrole N-H typically becomes more deshielded (as is seen for **5** in Table 2), an indication possibly of a conformational change that moves the N-H . In **1** and **2**, however, the pyrrole N-H is not as deshielded as in **5**, suggesting perhaps that the bulky C(10) substituents act to stabilize the ridge-tile conformation.

The corresponding dimethyl ester spectra in CDCl_3 of **3** and **4** are very similar to those of **6** (Table 3), except for the dipyrinone N-Hs . The lactam N-Hs are more shielded in **3** and **4** than in **6**.

The N-H chemical shifts of rubin acids and their esters are typically very similar in $(\text{CD}_3)_2\text{SO}$, cf **5** (Table 2) and **6** (Table 3). Thus, when bilirubins are esterified (*e.g.*, **6**, Table 3), or when the propionic acids are relocated away from C(8) and C(12) or replaced by simple alkyl groups, the pyrrole N-Hs are

TABLE 3. $^1\text{H-NMR}$ Chemical Shifts^a of Rubin Dimethyl Esters: **3** (X= *t*-butyl), **4** (X= Adamantyl), **6** (X= H) in CDCl_3 and $(\text{CD}_3)_2\text{SO}$.



Hydrogen Position	Chemical Shift in $(\text{CD}_3)_2\text{SO}$			Chemical Shift in CDCl_3		
	3	4	6	3	4	6
21,24 NH	9.41	9.33	9.78	9.71	9.70	10.44
22,23 NH	9.73	9.73	10.41	8.25-8.75	8.25-8.75	10.28
5,15 =CH-	5.96	5.99	5.92	5.83	5.85	5.98
10 CH ₂ CH	4.04	3.88	4.13	4.18	4.05	4.05
10 ¹ CH ₃	0.99	—	—	1.14	—	—
10 ² CH ₂	—	1.60	—	—	1.62	—
10 ³ CH	—	19.95	—	—	2.02	—
10 ⁴ CH ₂	—	1.60	—	—	1.62	—
8 ¹ ,12 ¹ CH ₂	2.61 ^b	2.65 ^b	2.88 ^c	2.82 ^b	2.85 ^b	2.52 ^c
8 ² ,12 ² CH ₂	2.11 ^b	2.20 ^b	2.49 ^c	2.49 ^b	2.50 ^b	2.25 ^c
7 ¹ ,13 ¹ CH ₃	2.02	2.06	2.16	2.14	2.16	2.06
3 ¹ ,17 ¹ CH ₃	1.92	1.96	1.93	1.56	1.72 1.70	1.95
2 ¹ ,18 ¹ CH ₃	1.74	1.77	1.54	1.36	1.64	1.77
8 ⁴ ,12 ⁴ OCH ₃	3.53	3.58	3.52	3.73	3.76	3.52

^a Run at 4×10^{-3} M concentration of pigment at 22°C; δ , ppm downfield from $(\text{CH}_3)_4\text{Si}$. ^b t, J= 7.80 Hz; ^c t, J= 7.50 Hz.

found near 10.3 ppm in $(\text{CD}_3)_2\text{SO}$.^{19,20} In CDCl_3 , the ester pyrrole N-H is also often deshielded to ~10.3 ppm (from ~9.2 ppm in bilirubin).^{19,20} This is because the esters in CDCl_3 adopt a more helical shape as they relinquish acid to dipyrinone hydrogen bonding (Fig. 2A) in favor of dipyrinone to dipyrinone intermolecular hydrogen bonding (Fig. 2B).

While the $^1\text{H-NMR}$ spectra for the core C-H signals of dimethyl esters **3** and **4** are similar to those of the parent (**6**), in both $(\text{CD}_3)_2\text{SO}$ and CDCl_3 , there is no signal doubling. Especially notable differences may be seen in the N-H resonances (Table 3). The lactam and pyrrole N-Hs are more shielded in **3** and **4** than in **6**, with the pyrrole N-Hs being especially strongly shielded in CDCl_3 — to values at higher field even than those of the corresponding acids, **1** and **2** (Table 2). The data seem to suggest ridge-tile conformations for **3** and **4**, attributable to geometric constraints imposed by the bulky C(10) *tert*-butyl and adamantyl groups.

Additional evidence on intramolecular hydrogen bonding between propionic acid (or ester) and dipyrinone groups in **1-6** can be elicited from an examination of coupling constants. It may be noted that vicinal coupling in the propionic acid ethylene ($-\text{C}_\beta\text{H}_2-\text{C}_\alpha\text{H}_2-\text{CO}_2\text{R}$) follows an A_2B_2 pattern of two triplets for all of the ester data of Table 2 and for the acid data only in $(\text{CD}_3)_2\text{SO}$ (Table 1). These data are consistent with relatively free segmental motion in these chains, as might attend limited or no hydrogen bonding with the carboxylic acid or ester groups. The situation is very different for acids **1**, **2** and **5** in CDCl_3 solvent. Here, an ABCX pattern (ddd) is exhibited by each $-\text{C}_\beta\text{H}_2-\text{C}_\alpha\text{H}_2-\text{CO}_2\text{R}$ segment.

Analysis of the vicinal H|H coupling constants in the propionic acid chains of **1**, **2** and **5** (Table 4) provides strong supporting experimental evidence for folded ridge-tile structures, as in Figure 1B. In CDCl_3 solvent, the well-defined ABCX coupling pattern is characteristic of restricted mobility⁶ in the

TABLE 4. $^1\text{H-NMR}$ Chemical Shifts^a and Coupling Constants^b for the Propionic Acid $-\text{C}_\beta\text{H}_\text{A}\text{H}_\text{X}-\text{C}_\alpha\text{H}_\text{B}\text{H}_\text{C}-\text{CO}_2\text{H}$ Segments in CDCl_3 at 22°C.

Pig-ment	$\beta\text{-CH}_2$		$\alpha\text{-CH}_2$		$\beta'\text{-CH}_2$		$\alpha'\text{-CH}_2$	
	H_X	H_A	H_B	H_C	$\text{H}_{\text{X}'}$	$\text{H}_{\text{A}'}$	$\text{H}_{\text{B}'}$	$\text{H}_{\text{C}'}$
1 δ : R= <i>t</i> Bu	3.07	2.53	2.78	2.87	3.45	2.65	2.78	3.03
	J_{BX} 13.00 J_{CX} 3.00 J_{AX} -15.00	J_{AB} 2.50 J_{AC} 4.50 J_{AX} -15.00	J_{AB} 3.00 J_{BX} 4.50 J_{BC} -17.50	J_{AC} 13.00 J_{CX} 2.50 J_{BC} -17.50	$J_{\text{B}'\text{X}'}$ 12.50 $J_{\text{C}'\text{X}'}$ 3.00 $J_{\text{A}'\text{X}'}$ -14.50	$J_{\text{A}'\text{B}'}$ 2.50 $J_{\text{A}'\text{C}'}$ 4.50 $J_{\text{A}'\text{X}'}$ -14.50	$J_{\text{A}'\text{B}'}$ 3.00 $J_{\text{B}'\text{X}'}$ 4.50 $J_{\text{B}'\text{C}'}$ -19.00	$J_{\text{A}'\text{B}'}$ 12.50 $J_{\text{C}'\text{X}'}$ 2.50 $J_{\text{B}'\text{C}'}$ -19.00
2 δ : R=Ada	3.08	2.54	2.82	2.88	3.64	2.70	2.82	3.04
	J_{BX} 13.00 J_{CX} 2.50 J_{AX} -15.00	J_{AB} 2.50 J_{AC} 4.50 J_{AX} -15.00	J_{AB} 2.50 J_{BX} 4.50 J_{BC} -18.25	J_{AC} 13.00 J_{CX} 2.50 J_{BC} -18.25	$J_{\text{B}'\text{X}'}$ 12.25 $J_{\text{C}'\text{X}'}$ 2.50 $J_{\text{A}'\text{X}'}$ -14.25	$J_{\text{A}'\text{B}'}$ 2.50 $J_{\text{A}'\text{C}'}$ 4.50 $J_{\text{A}'\text{X}'}$ -14.25	$J_{\text{A}'\text{B}'}$ 2.50 $J_{\text{B}'\text{X}'}$ 4.50 $J_{\text{B}'\text{C}'}$ -19.00	$J_{\text{A}'\text{C}'}$ 22.75 $J_{\text{C}'\text{X}'}$ 2.50 $J_{\text{B}'\text{C}'}$ -19.00
5 δ : R=H	2.99	2.54	2.78	2.89				
	J_{BX} 13.50 J_{CX} 2.60 J_{AX} -15.00	J_{AB} 2.60 J_{AC} 4.60 J_{AX} -15.00	J_{AB} 4.60 J_{BX} 2.60 J_{BC} -18.70	J_{AC} 13.50 J_{CX} 2.60 J_{BC} -18.70				

^a δ , ppm downfield from $(\text{CH}_3)_4\text{Si}$. ^b J in Hertz from 500 MHz spectra.

$-\text{CH}_A\text{H}_X\text{CH}_B\text{H}_C-\text{COOH}$ segment which is constrained to adopt a fixed staggered geometry (Table 4) due to strong intramolecular hydrogen bonding, *e.g.*, Fig. 1B. On the other hand, the less complicated A_2B_2 pattern found in $(\text{CD}_3)_2\text{SO}$ solvent (Table 2) indicates more motional freedom in the propionic acid segment, whose CO_2H groups are linked to the dipyrinones via bound solvent molecules.^{6c}

The stereochemical conclusions reached above were confirmed by $^1\text{H}\{^1\text{H}\}$ -homonuclear Overhauser effect (NOE) measurements in CDCl_3 (Figure 3). The *syn-Z*-dipyrinone conformation is confirmed by moderately strong NOEs between: (i) the pyrrole and lactam NHs within individual dipyrinones and (ii) the vinylic hydrogens at C(5) and C(15) and the pyrrole methyls at C(7) and C(13), and the lactam methyls at C(3) and C(17). Significantly, NOEs are observed between CO_2H and lactam NH, as anticipated from intramolecularly hydrogen-bonded conformations. NOEs are also observed between the *tert*-butyl methyl(s) and the $\beta\text{-CH}_X$, at 3.45 ppm (Table 2) in **1**. Taken collectively, the NMR data support a fixed staggered conformation of the propionic acid segment and intramolecularly hydrogen-bonded ridge-tiles for **1**, **2** and **5**.

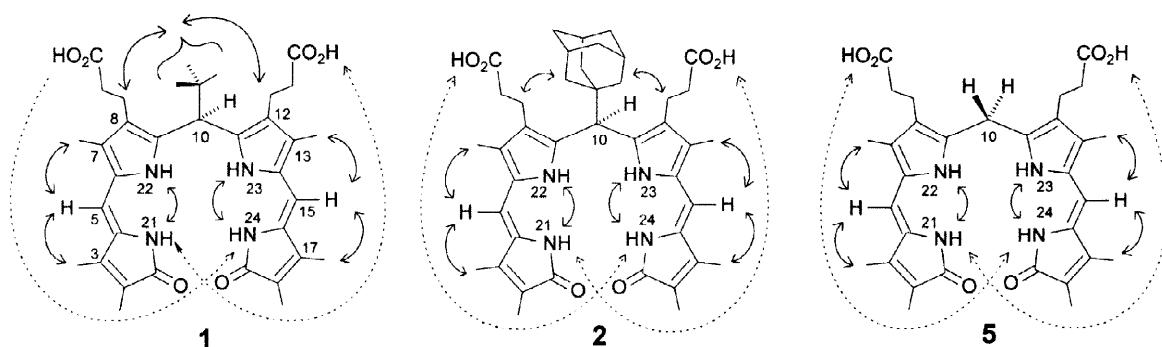


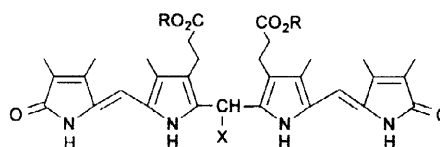
FIGURE 3. $^1\text{H}\{^1\text{H}\}$ -homonuclear Overhauser effects (NOEs) found in **1** and **2** and their parent (**5**) in CDCl_3 are shown by solid, double-headed curved arrows. Significant, albeit weak, NOEs are found between the CO_2H protons and the lactam N-H protons at N(21) and N(24), as indicated by dashed arrows.

UV-Visible Spectral Analysis and Conformation from Exciton Coupling. Further evidence on intramolecular hydrogen bonding comes from solvent-dependent UV-visible spectra. Over a wide range of solvents with varying polarity and hydrogen bonding ability (benzene, chloroform, methanol and dimethylsulfoxide), the UV-visible spectra of mesobilirubin-XIII α (a well-studied analog of **5**, with ethyl groups at C(3) and C(17)) change very little, with λ^{max} being near 430 nm and λ^{sh} near 395 nm^{19b,21} — corresponding to the two exciton components from electric transition dipole-dipole interaction of the two proximal dipyrinone chromophores approximately 90° apart (as in Figure 1).^{4,22,23} Since mesobilirubin-XIII α and **5** are known from NMR studies to adopt the intramolecularly hydrogen bonded conformation of Figure 1 in CDCl_3 solvent and a similar conformation in $(\text{CD}_3)_2\text{SO}$ solvent,^{4,6,10,18} it might be argued that a UV-visible exciton couplet with $\lambda^{\text{max}} \sim 430$ nm, $\lambda^{\text{sh}} \sim 395$ nm can be taken as an indicator of a folded (but not necessarily hydrogen-bonded) conformation akin to that of Figure 1. The UV-visible spectra of **1** and **2** (Table 5) are very much alike but differ somewhat from those of **5**, especially in $(\text{CH}_3)_2\text{SO}$ solvent, where

λ^{\max} is at 389 nm, with λ^{sh} near 411–416 nm for **1** and **2**. In contrast, for **5** λ^{\max} is at 426 nm, with λ^{sh} near 390 nm. The data for **1** and **2** in $(\text{CH}_3)_2\text{SO}$ are consistent with a more helical folded conformation, one with a smaller interplanar angle. The spectral data in CHCl_3 and other non-polar solvents support the intramolecularly hydrogen bonded ridge-tile in **1**, **2** and **5**.

UV-visible spectral data for dimethyl esters **3**, **4** and **6** show a different solvent dependence. Spectra in nonpolar solvents are quite similar to those of mesobilirubin-XIII α dimethyl ester, which typically exhibits a strong solvent, concentration and temperature dependence due to formation of dimers^{2,24} in non-polar solvents such as benzene and chloroform. This results in spectra with a narrow bandwidth intense absorption at λ^{\max} near 380 nm and weak shoulder at λ^{sh} near 430 nm.^{19b,21} In more polar solvents such as CH_3OH and $(\text{CH}_3)_2\text{SO}$ the solutions are largely monomeric, and the UV-visible spectra are rather similar to those of the parent acids in these solvents.

TABLE 5. Solvent Dependence of UV-Visible Spectra^a of Rubins (R=H): **1** (X= *t*-butyl), **2** (X= 1-Adamantyl) and **5** (X= H) and Their Corresponding Dimethyl Esters (R= CH_3): **3**, **4** and **6**.



Solvent	$\epsilon^{\max} (\lambda^{\max})$ of Acids			$\epsilon^{\max} (\lambda^{\max})$ of Dimethyl Esters		
	1	2	5	3	4	6
C_6H_6	47700 (421)	57384 (437) 54542 (421) ^{sh}	Insol.	40554 (381) 18835 (423) ^{sh}	44874 (382) 26434 (410) ^{sh}	52700 (384)
CH_2Cl_2	48300 (420) ^{sh} 50020 (433)	48458 (417) ^{sh} 51838 (433)	51000 (427)	40275 (381) 24825 (409) ^{sh}	49033 (381) 26901 (418) ^{sh}	57600 (379)
CHCl_3	48510 (422) ^{sh} 50500 (436)	49722 (417) ^{sh} 52755 (438)	58000 (431)	39631 (389) ^{sh} 52406 (401)	44484 (399) 25780 (423) ^{sh}	48400 (381) 36600 (411) ^{sh}
$(\text{CH}_3)_2\text{CO}$	47590 (424)	29907 (426)	Insol.	38512 (380) 27288 (408) ^{sh}	43440 (380) 33126 (405) ^{sh}	47000 (381) 34000 (427) ^{sh}
CH_3OH	38030 (396) 37855 (416) ^{sh}	31856 (396) 30292 (415) ^{sh}	Insol.	36794 (394) 35675 (414) ^{sh}	41401 (393) 39401 (415) ^{sh}	47400 (427)
$(\text{CH}_3)_2\text{SO}$	41300 (416) ^{sh} 41590 (389)	46167 (389) 35454 (411) ^{sh}	57300 (426)	38269 (388) 33438 (415) ^{sh}	45016 (387) 38538 (407) ^{sh}	32500 (389) ^{sh} 43500 (428)

^a ϵ^{\max} and ϵ^{sh} in $\text{L} \cdot \text{mol}^{-1} \cdot \text{cm}^{-1}$ at (λ in nm) for 10^{-5} M solutions.

Conformation from Molecular Dynamics. Like bilirubin (Fig. 1) **1**, **2** and **5** may be viewed as two-blade molecular propellers, where the blades consist of dipyrinones connected to a CH_2 or CHR at C(10). As such, they are related to the simpler propeller, diphenylmethane, studied and analyzed by Mislow *et al.*²⁵ Force-field analyses suggest that diphenylmethane prefers the C_{2v} gable conformation over the C_2 propeller geometry, but *tert*-butyl and 1-adamantyl diphenylmethane prefer the C_2 or propeller conformation by ~ 3 kcal/mole (Fig. 4). Like a *gem*-dimethyl,¹⁰ apparently, the *tert*-butyl and adamantyl groups have a moderate stabilizing effect on the C_2 conformation. Such groups might also be expected to stabilize the C_2 conformation in other molecular propellers, such as the C(10) *tert*-butyl and C(10) adamantyl analogs of bilirubin (**1** and **2**, respectively).

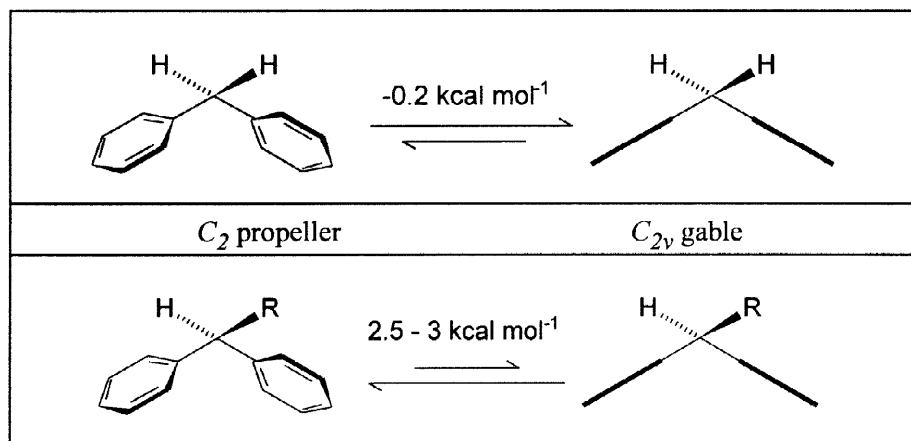


FIGURE 4. (Upper) Diphenylmethane conformations, with the C_{2v} gable geometry being slightly favored over the C_2 propeller. (Lower) *tert*-Butyl and 1-adamantyl diphenylmethane conformations, with the C_2 propeller geometry more substantially favored.

In the tetrapyrrole analogs (**1**, **2** and **5**) of diphenylmethane, the longer dipyrinone blades have at least one degree of conformational freedom not available in the simpler systems: the potential for curvature within the blades by twisting the C(5)-C(6) or C(14)-C(15) carbon-carbon single bonds. However, the conformational possibilities within the dipyrinone blades are severely limited, as judged from earlier work involving both experiment² and CNDO/2-based force-field calculations,^{2,26} which indicate a strong preference for the *syn*-periplanar or *syn*-clinal conformations (Fig. 2). The *syn*-periplanar conformation with C(5)-C(6) or C(14)-C(15) torsion angles 0-20° predominates in crystalline bilirubin and in dipyrinone hydrogen-bonded *dimers*. *Syn*-clinal conformations, with C(5)-C(6) torsion angles 20-50° are favored by *monomeric* dipyrinones with unsubstituted N-H groups. In bilirubins, differences in shape brought about by twisting the blades are small compared with conformations generated through rotations of the dipyrinone blades about their C(9)-C(10) and C(10)-C(11) bonds (Fig. 1).

Rotations about the C(9)-C(10) and C(10)-C(11) carbon-carbon single bonds sweep the dipyrinone blades through large spatial distances and produce a wide variety of rather different and distinctive conformational structures. At the two extremes are the planar or nearly planar porphyrin-like and extended conformations of Figs. 1A and C. (The porphyrin-like conformation is designated the $\phi_1 = \phi_2 \sim 0^\circ$ conformer; the extended conformation can be designated the $\phi_1 = \phi_2 \sim 180^\circ$ conformer.) Lying in between these two planar conformations are a very large number of non-planar conformations, each of which has a non-superimposable mirror image (as in the $\phi_1 = \phi_2 = 90^\circ$ and $\phi_1 = \phi_2 = -90^\circ$ gabled conformers). However, not all of the conformers are expected to be equal in energy.^{2,4,26} For example, in the extended conformation of Fig. 1C the propionic acid groups are severely buttressed against one another; and in the porphyrin-like conformation of Fig. 1A, destabilizing non-bonded steric interactions arise between the pyrrole N-H groups and the lactam carbonyl groups. These two conformers might thus be expected to be less stable than any of the non-planar conformations in which non-bonding repulsions are minimized.

An examination of CPK-space filled models allows one to see the cited elements of conformational destabilization, and molecular mechanics force-field calculations place those observations on a quantitative basis. Using the SYBYL force-field program on an Evans and Sutherland ESV-10 graphics workstation, conformational energy maps for **1**, **2** and **5** were generated. The map for **1** (Fig. 5) is nearly identical to that of **2**, and both are very similar to those of **5**,^{10b} bilirubin⁴ and mesobilirubin-XIII α .⁴ For **1** the clearly

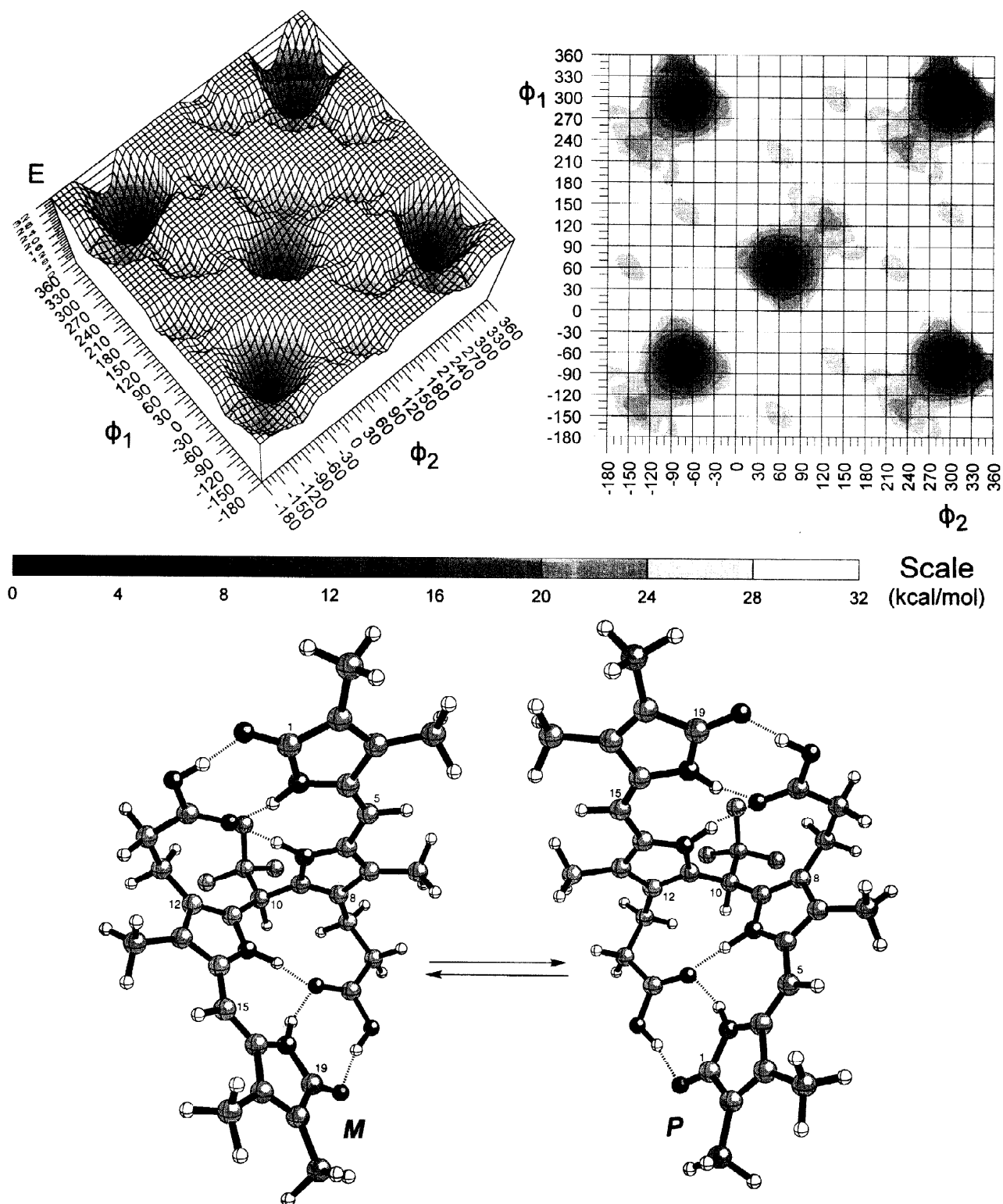
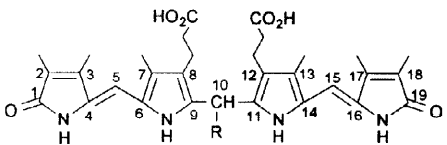


FIGURE 5. (Upper) Potential energy surface (left) and contour map (right) for conformations of **1** generated by rotating its two dipyrinone groups independently about the C(9)-C(10) and C(10)-C(11) bonds (ϕ_1 and ϕ_2 , respectively). The energy scale (bottom) is in kcal/mole. Isoenergetic global minima (set to 0 kcal/mole) are found near $(\phi_1, \phi_2) = (60^\circ, 60^\circ)$ (*P*-chirality) and near $(\phi_1, \phi_2) = (-60^\circ, -60^\circ), (-60^\circ, 300^\circ), (300^\circ, -60^\circ), (300^\circ, 300^\circ)$ (*M*-chirality). Local minima (20 kcal/mole above the global minima) are found near the $(60^\circ, 60^\circ)$ global minimum at $(\phi_1, \phi_2) = (60^\circ, 220^\circ), (220^\circ, 60^\circ), (-60^\circ, 140^\circ)$ and $(140^\circ, -60^\circ)$. (Lower) Interconverting ball and stick conformational representations for the *M* and *P* helical global minima. (Hydrogens on the *tert*-butyl groups are removed for clarity.)

TABLE 6. Influence of C(10) Substitution on Selected Molecular Parameters for Energy-Minimum Conformations of 10-*tert*-Butyl and 10-(1-Adamantyl) Rubins Determined by Molecular Dynamics Calculations.

Torsion and Interplanar Angles (°) and Nonbonded Distances (Å)			
	5 R=H	1 R= <i>tert</i> -Butyl	2 R=1-Adamantyl
ϕ_1 (22-9-10-11) ^b	59	63 (220) ^g	60 (220) ^g
ϕ_2 (9-10-11-23) ^b	59	52 (60) ^g	60 (60) ^g
ψ_1 (4-5-6-22) ^c	17	15 (35) ^g	16 (34) ^g
ψ_2 (23-14-15-16) ^c	-8.6	-4.6 (121) ^g	-3.6 (120) ^g
(21-4-5-6) ^d	1.5	0.9 (-3.0) ^g	0.7 (-3.4) ^g
(14-15-16-24) ^d	-0.7	-0.6 (0.8) ^g	-0.8 (-3.0) ^g
θ (dipyrinone) ^e	88	87 (68) ^g	90 (77) ^g
θ (pyrrole) ^e	87	86 (78) ^g	88 (80) ^g
d(C=O ... O=C) ^f	11	11 (13.3) ^g	11 (13.5) ^g
d(vertical)	5.6	5.4 (6.0) ^g	5.4 (6.5) ^g

^a Using Sybyl ver. 6.0 for the Evans & Sutherland ESV-10⁺ workstation, ref. 4. ^b Values would be ~0° for the porphyrin conformation, ~60° for the ridge-tile conformation and ~180° for the linear conformation. ^c Indicates distortion from a planar dipyrinone, where $\psi \sim 0^\circ$. ^d Indicates twist from 0° of C=C. ^e Interplanar dihedral angle using the average plane of each dipyrinone or the dihedral angle of the two pyrroles adjacent to C(10). ^f Dipyrinone oxygen-oxygen nonbonded distance and the vertical distance determined from one dipyrinone oxygen to the average plane of the second dipyrinone. ^g Parameters for nearest local minimum lying some 15-20 kcal/mole above the global minimum.

separated local minima lie some 15-20 kcal/mole above the global minima. In all of these maps, isoenergetic global minima are clearly located near ($\phi_1 = \phi_2 \sim 60^\circ$), ($\phi_1 = \phi_2 \sim -60^\circ$), ($\phi_1 = \phi_2 \sim 300^\circ$), ($\phi_1 \sim 300^\circ$, $\phi_2 \sim -60^\circ$), and ($\phi_1 \sim -60^\circ$, $\phi_2 \sim 300^\circ$). Each global minimum lies as a deep depression in a canyon with steeply rising walls. Local minima lie in significantly higher energy valleys. Even in the absence of hydrogen bonding the global minimum-energy conformation has a ridge-tile shape that places the propionic acid carboxyl groups in a position ideal for hydrogen bonding to the opposing dipyrinone lactam carbonyl and N-H groups and the pyrrole N-H group. Hydrogen bonding sharply lowers the global energy minima and thus acts as a powerful conformation-stabilizing force — not available to most of the other tetrapyrrole conformers which form the conformational energy map.

The global minimum conformations of Fig. 5 correspond to either of two unique 3-dimensional conformers, *M* and *P* which appear to play a central role in explaining many of the properties of bilirubin pigments. The global minimum ridge-tile conformers found in our force-field calculations of bilirubin are nearly identical to those seen in its X-ray crystal structures.²⁷ In those conformations (Fig. 1B), the polar propionic acid carboxyl groups are sequestered internally, thus rendering the pigment lipophilic. It may be seen that the *M* and *P* conformers of Fig. 5 are mirror image structures: *P* corresponds to the global minimum (Fig. 5) at ($\phi_1 = \phi_2 \sim 60^\circ$), *M* corresponds to global minima at ($\phi_1 = \phi_2 \sim -60^\circ$), ($\phi_1 = \phi_2 \sim 300^\circ$),

($\phi_1 \sim -60^\circ$, $\phi_2 \sim 300^\circ$) and ($\phi_1 \sim 300^\circ$, $\phi_2 \sim -60^\circ$). The *M* and *P* conformational enantiomers interconvert by breaking the minimum number of hydrogen bonds while rotating the dipyrinones about ϕ_1 and ϕ_2 and remaking the hydrogen bonds. From an examination of Fig. 5, two distinct low energy interconversion pathways may be charted from *P* to *M*: (1) A route from ($\phi_1 = \phi_2 \sim 60^\circ$) \rightarrow ($\phi_1 \sim 0^\circ$, $\phi_2 \sim 90^\circ$) \rightarrow ($\phi_1 \sim -40^\circ$, $\phi_2 \sim 100^\circ$) \rightarrow ($\phi_1 \sim -40^\circ$, $\phi_2 \sim 130^\circ$) \rightarrow ($\phi_1 \sim -60^\circ$, $\phi_2 \sim 180^\circ$) \rightarrow ($\phi_1 \sim -80^\circ$, $\phi_2 \sim 180^\circ$) and down to ($\phi_1 = -60^\circ$, $\phi_2 = 300^\circ$), with an activation barrier of ~ 30 kcal/mole in the case of **1** or **2** (vs. ~ 19 kcal/mole for **5**). (2) A route from ($\phi_1 = \phi_2 \sim 60^\circ$) \rightarrow ($\phi_1 \sim 0^\circ$, $\phi_2 \sim 90^\circ$) \rightarrow ($\phi_1 \sim -40^\circ$, $\phi_2 \sim 100^\circ$) \rightarrow ($\phi_1 \sim -90^\circ$, $\phi_2 \sim 100^\circ$) \rightarrow ($\phi_1 \sim -100^\circ$, $\phi_2 \sim 20^\circ$) \rightarrow ($\phi_1 \sim -100^\circ$, $\phi_2 \sim -60^\circ$) and down to ($\phi_1 = \phi_2 \sim -60^\circ$), with a barrier of ~ 32 kcal/mole in the case of **1** or **2** (and ~ 22 kcal/mole for **5**).

The high energy valleys (isolated local minima) near the global minima of **1** or **2** (Fig. 5) correspond to structures shown in Fig. 6. Like the global minimum, the local minimum conformations are also stabilized by intramolecular hydrogen bonds, accommodated by the dipyrinones twisting out of planarity. The latter is accommodated by rotations in the propionic acid chain that bring the β -CH₂ groups forward (required at some point along the *P* \rightleftharpoons *M* interconversion path), and by slight twisting about C(5)-C(6) and C(14)-C(15) in the dipyrinones. Nonbonded steric repulsions involving the *tert*-butyl or adamantyl groups are thus somewhat relieved at the expense of longer (less stable) hydrogen bonds.

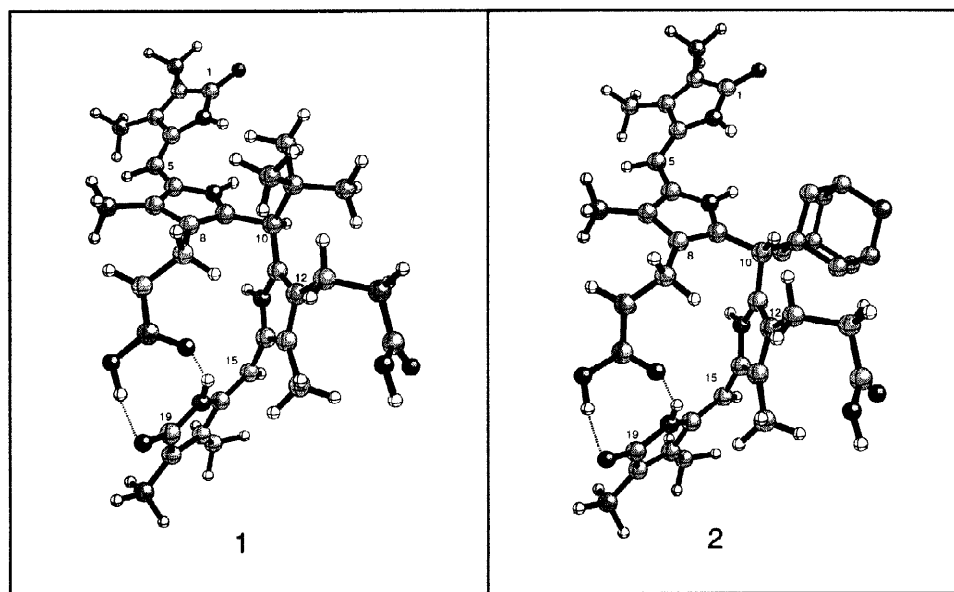


FIGURE 6. Ball and stick conformations of local minima of **1** and **2** that lie ~ 20 and ~ 15 kcal/mole, respectively, above the global minima. In these local minima, $\phi_1 \sim 60^\circ$, $\phi_2 \sim 200^\circ$. Adamantane hydrogens are removed for clarity.

Conformational Enantiomerism and Induced Circular Dichroism. In a nonpolar, aprotic solvent such as chloroform, the conformational equilibrium between bilirubin enantiomers can be displaced from 1:1 by the addition of a chiral recognition agent.^{22a} Similarly, for bilirubin analogs **1**, **2** and **5** in CHCl₃ an induced CD may be observed in the presence of quinine (Fig. 7). At a molar ratio of alkaloid:pigment of $\sim 300:1$, the Cotton effect intensities reach a maximum for **5**, giving an intense bisignate CD ($\Delta\epsilon_{386}^{\max} - 83$, $\Delta\epsilon_{386}^{\max} + 52$), of exactly the same signed order and nearly the same magnitude as that seen for bilirubin or mesobilirubin-XIII α .^{22a} With **1** and **2**, however, the Cotton effect intensities are reduced by nearly an order of magnitude. Whether this reflects ineffective complexation/recognition or an altered pigment conformation is not immediately clear. However, it is clear that although **1** and **2** behave qualitatively like **5**,

they do not behave exactly alike — evidence that the C(10) *tert*-butyl and adamantyl groups exert an important stereochemical effect.

When human serum albumin (HSA) is used as the chiral complexation agent, however, aqueous solutions (pH 7.4 Tris buffer) of **5** behave very similarly to those of bilirubin or mesobilirubin-XIII α ,²⁸ exhibiting moderately intense bisignate CD curves ($\Delta\epsilon_{426}^{\max} +56$, $\Delta\epsilon_{380}^{\max} -23$) due to enantioselective chiral complexation of the pigment by the protein. For solutions of **1** and **2** with HSA, however, the magnitude of the CD Cotton effects are considerably lowered and the signs are reversed (**1**: $\Delta\epsilon_{430}^{\max} -22$, $\Delta\epsilon_{395}^{\max} +10$ and **2**: $\Delta\epsilon_{430}^{\max} -23$, $\Delta\epsilon_{370}^{\max} +11$) while maintaining clearly defined bisignate shapes (Fig. 8). The data indicate that the conformation of **1** and **2** on HSA is probably different from that of **5** on HSA. Surprisingly the data indicate a preference for the opposite helical conformation in **1** and **2** relative to **5**.

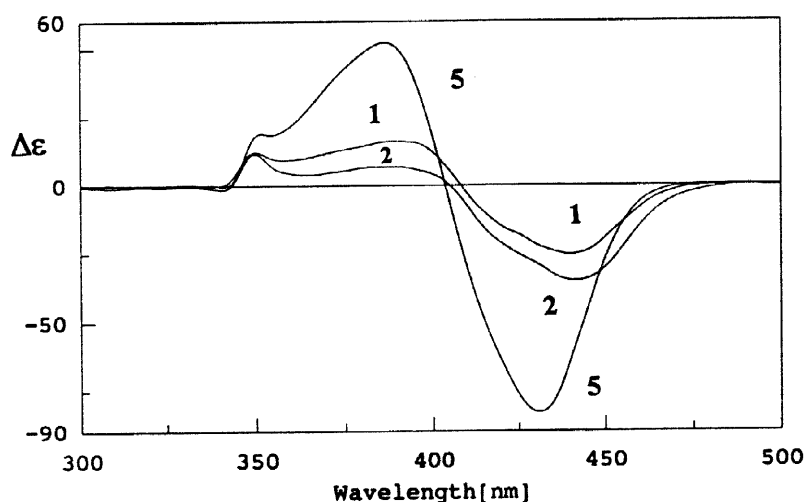


FIGURE 7. Circular dichroism spectra of 2.0×10^{-5} M *tert*-butyl rubin (**1**), adamantyl rubin **2** and the parent rubin (**5**) in CHCl_3 in the presence of 6.0×10^{-3} M quinine at 22°C . The compound numbers are indicated on each CD curve.

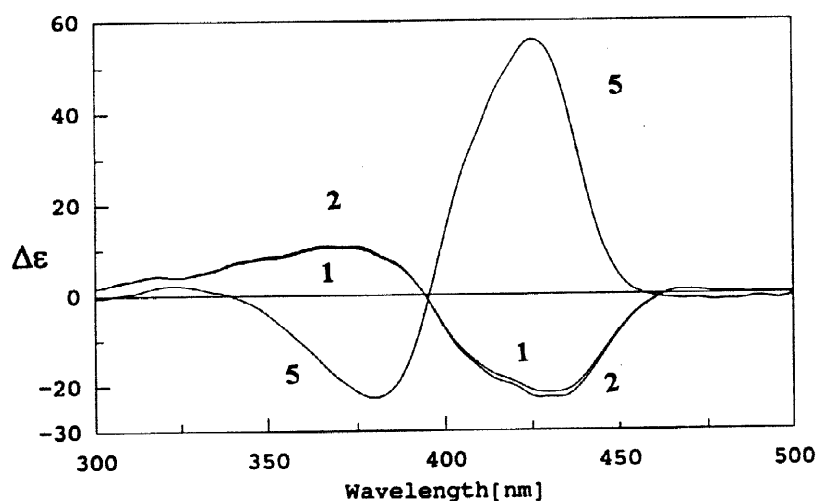
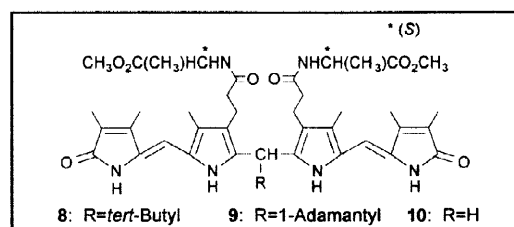


FIGURE 8. Circular dichroism spectra of 2.0×10^{-5} M *tert*-butyl rubin (**1**), adamantyl rubin **2** and the parent rubin (**5**) in the presence of 4.0×10^{-5} M HSA in pH 7.4 Tris buffer at 22°C . The compound numbers are indicated on each CD curve.

When the chiral agent is covalently attached to the pigment, as in propionamide derivatives with amino acid esters, CD may also be observed. Thus, following conversion of **1** and **2** to their bis-amides (**8** and **9**, respectively) with (*S*)-alanine methyl ester by the Shioiri procedure used previous-



ly,^{10b,29} the CD spectra of the optically active pigment amides were determined (Fig. 9) to reveal very weak CDs — as contrasted with the parent amide (**10**). Interestingly, although ¹H-NMR (in which the propionamide O=C–N–H is found to be strongly deshielded) indicates a high probability of intramolecular hydrogen bonding in **10** (Table 7), in **8** and **9** it appears not to be involved in hydrogen bonding. Similarly, the dipyrinone NH chemical shifts of **10** differ significantly from those of **8** and **9**, with the latter suggesting weaker hydrogen bonding. Thus, it would seem that whereas the conformation of **10** retains its bilirubin-like hydrogen bonded ridge-tile structure, the conformation of **8** or **9** is not quite the same. In a behavior similar to that of the 10,10-dimethyl analog,¹⁰ the bulky C(10) alkyl groups play a major role in weakening intramolecular hydrogen bonding in bis-amide **8** or **9** but are apparently less influential in the parent diacids (**1** and **2**). The reasons for the difference in behavior are not entirely clear, but they may relate to the longer length of the O–H vs N–H bond in a more open ridge-tile conformation in **8** and **1** (or **9** and **2**) vs that of **10** and **5**, where intramolecular hydrogen bonding is accessible in both the acid and amide. Thus, the NMR data and the CD data (Table 8) suggest very weak conformational selection of the *P*-helicity diastereomers in **8** and **9**, and 1–2 orders of magnitude stronger selection of the *P*-helicity diastereomer in **10**.

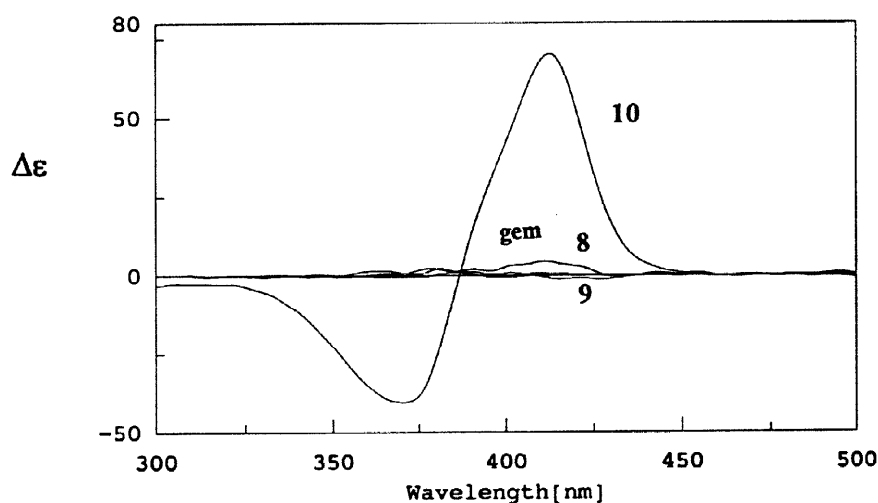


FIGURE 9. Circular dichroism spectra of 1.0×10^{-5} M (*S*)-alanyl methyl ester rubin bis-amides with C(10) *tert*-butyl (**8**), C(10) adamantyl (**9**) and the parent (**10**) in CH_3CN solvent at 22°C. The compound numbers are indicated on the CD curves. For comparison, the CD of the 10,10-dimethyl analog is included (gem).

TABLE 7. ¹H-NMR Chemical Shifts^a of Amide and Pyrrole N–Hs of the *S*-Alanine Methyl Ester Bis-amides (**8–10**) of **1**, **2** and **5**, respectively, in CDCl_3 at 22°C.

Pigment	Lactam	Pyrrole	Alanine
8	9.63 9.78	8-9 (v.br)	7.32 (syn) 6.90 (anti)
9	9.59 9.75	8-9 (v.br)	7.30 (syn) 6.95 (anti)
10	11.70	10.62	10.25 (syn)

^a δ , ppm downfield from $(\text{CH}_3)_4\text{Si}$.

TABLE 8. Circular Dichroism and UV-Visible Spectral Data^a for the Bis-Amides **8-10** of **1**, **2** and **5**, respectively, with *S*-Alanine Methyl Ester at 22°C.

Solvent	Pigment	Circular Dichroism			UV-Visible
		$\Delta\epsilon_{\max}(\lambda_1)$	λ at $\Delta\epsilon=0$	$\Delta\epsilon_{\max}(\lambda_2)$	$\epsilon_{\max}(\lambda)$
CH ₂ Cl ₂	8	-0.7 (433)	422	+1.9 (383)	54,600 (386)
	9	-0 (440)	—	-3.1 (374)	45,900 (387)
	10	+32 (415)	388	-20 (375)	41,400 (406)
CH ₃ CN	8	-0.4 (431)	422	+2.0 (381)	57,500 (380)
	9	-1.5 (427)	392	+2.0 (381)	53,300 (380)
	10	+69 (414)	387	-41 (373)	43,000 (414)
(CH ₃) ₂ CO	8	-1.4 (432)	396	+1.7 (380)	54,000 (383)
	9	-5.5 (413)	395	+4.8 (377)	44,500 (383)
	10	+67 (416)	388	-39 (374)	36,500 (416)
CH ₃ OH	8	-1.1 (410)	402	+2.1 (386)	49,200 (393)
	9	-4.0 (415)	392	+3.3 (374)	45,700 (395)
	10	+52 (420)	390	-28 (380)	46,000 (418)
(CH ₃) ₂ SO	8	-4.5 (423)	395	+4.1 (380)	51,650 (389)
	9	-5.4 (420)	393	+3.4 (363)	51,400 (388)
	10	+10 (420)	389	-1.7 (379)	47,000 (425)

^a $\Delta\epsilon$ and ϵ in L · mole⁻¹ · cm⁻¹ and λ in nm; ^b For 1×10^{-5} M pigment solutions.

Concluding Comments

Intramolecular hydrogen bonding between the propionic acid CO₂H and dipyrinone groups is known to be a dominant, conformation-stabilizing force in bilirubin. In the current study, the influence of a single *tert*-butyl or adamantyl substituent at C(10) in a bilirubin analog is evaluated. These bulky C(10) substituents lie at the ridge-tile seam and introduce an internal steric buttressing on the proximal (but not the distal) propionic acid chain thereby forcing a distortion in one-half of the ridge-tile conformation. The C(10) *tert*-butyl or adamantyl substituent raises the barrier to *M* ⇌ *P* conformational enantiomer inversion and also stabilizes the intramolecularly hydrogen bonded ridge-tile conformation.

Experimental

General Procedures. All ultraviolet-visible spectra were recorded on a Perkin-Elmer λ -12 spectrophotometer, and all circular dichroism (CD) spectra were recorded on a Jasco J-600 instrument. Nuclear Magnetic Resonance (NMR) spectra were obtained on GE QE-300 or GE GN-300 spectrometers operating at 300 MHz, or on a Varian Unity Plus 500 MHz spectrometer in CDCl₃ solvent (unless otherwise specified). Chemical shifts were reported in δ ppm referenced to the residual CHCl₃ ¹H signal at 7.26 ppm and ¹³C signal at 77.0 ppm. A *J*-modulated spin-echo experiment (*Attached Proton Test*) was used to assign ¹³C-NMR spectra. Melting points were taken on a MelTemp capillary apparatus and are uncorrected. Combustion analyses were carried out by Desert Analytics, Tucson, AZ. Analytical thin layer chromatography was carried out on J.T. Baker silica gel IB-F plates (125 μ layers). Flash column chromatography was carried out using Woelm silica gel F, thin layer chromatography grade. Radial chromatography was carried out on Merck Silica Gel PF₂₅₄ with gypsum

preparative layer grade, using a Chromatotron (Harrison Research, Inc., Palo Alto, CA). HPLC analyses were carried out on a Perkin-Elmer Series 4 high performance liquid chromatograph with an LC-95 UV-visible spectrophotometric detector (set at 410 nm) equipped with a Beckman-Altex ultrasphere-IP 5 μm C-1 8 ODS column (25 \times 0.46 cm) and a Beckman ODS precolumn (4.5 \times 0.46 cm). The flow rate was 1.0 mL/minute, and the elution solvent was 0.1 M di-*n*-octylamine acetate in 5% aqueous methanol pH 7.7, 31 °C). Spectral data were obtained in spectral grade solvents (Aldrich or Fisher). Pivaldehyde, adamantane, bromine, triethylamine, DDQ, trifluoroacetic anhydride, trifluoroacetic acid (TFA) L-alanine methyl ester hydrochloride and diphenylphosphoryl azide (DPPA) were from Aldrich. Dichloromethane, methanol, DMSO, formic acid, acetic acid, phosphorus pentoxide, and tetrahydrofuran were from Fisher.

10-*tert*-Butyl-8,12-bis-(2-carboxyethyl)-2,3,7,13,17,18-hexamethyl-1,10,19,21,23,24-hexahydro-1,19-dioxobilin (1). 3-Nor-neoxanthobilirubic acid **7** (548 mg, 2.00 mmole) was placed into a 25 mL round bottom flask along with a small magnetic stir bar. The flask was then fitted with a rubber septum and 6 mL of dichloromethane was added. After flushing the system with N_2 for several minutes, pivaldehyde (119 μL , 1.10 mmole) and TFA (500 μL) were added via a syringe. Upon addition of the acid, the mixture became homogeneous and reddish orange. It was allowed to stir under N_2 at room temperature for 8 hrs; then the dark solution was taken up in 100 mL of dichloromethane and washed with water and saturated aq. NaCl. After drying over anhydr. Na_2SO_4 , the solution was evaporated to give a dark solid, which was initially purified by flash-column chromatography on silica gel eluting with dichloromethane-methanol 100:2 (by vol). The resulting orange solid was further purified by radial chromatography, eluting with dichloromethane-methanol 100:2 (by vol) to afford 404 mg (66%) of the desired bright yellow pigment (**1**). It had mp 270 °C (dec); IR (KBr) ν : 3404, 2955, 1684, 1654, 1435, 1392, 1245, 1178, 940 cm^{-1} ; and $^1\text{H-NMR}$ and $^{13}\text{C-NMR}$ spectral data in Tables 1 and 2.

<i>Anal.</i> Calcd. for $\text{C}_{35}\text{H}_{44}\text{O}_6\text{N}_4$ (616.7):	C, 68.16; H, 7.19; N, 9.08.
Calcd. for $\text{C}_{35}\text{H}_{44}\text{O}_6\text{N}_4 \cdot \text{CH}_3\text{OH}$ (648.7):	C, 66.63; H, 7.46; N, 8.64.
Found:	C, 66.96; H, 7.50; N, 8.58.

10-*tert*-Butyl-8,12-bis-(2-methoxycarbonylethyl)-2,3,7,13,17,18-hexamethyl-1,10,19,21,23,24-hexahydro-1,19-dioxobilin (3). Excess ethereal diazomethane was added to a solution of **1** (100 mg) in 20 mL dry THF and allowed to stir at room temperature for *ca.* one hour. The solvents were allowed to evaporate leaving a yellow residue. Radial chromatography using dichloromethane-methanol 100:3 (by vol) gave 98.1 mg (94%) of the desired dimethyl ester (**3**). It had mp 210 °C (dec.); IR (KBr) ν : 3382, 2952, 2362, 1734, 1659, 1541, 1437, 1364, 1262, 1168, 579, 482 cm^{-1} ; and $^1\text{H-NMR}$ and $^{13}\text{C-NMR}$ spectral data in Tables 1 and 2. An analytical sample was prepared by the addition of hexane to a dichloromethane solution of the pigment followed by slow evaporation of the solvents under a stream of nitrogen. The resultant bright yellow crystals were filtered and dried over P_2O_5 in a drying pistol overnight.

<i>Anal.</i> Calcd. for $\text{C}_{37}\text{H}_{48}\text{O}_6\text{N}_4$ (644.8):	C, 68.92; H, 7.50; N, 8.69.
Found:	C, 68.99; H, 7.55; N, 8.42.

10-(1-Adamantyl)-8,12-bis-(2-carboxyethyl)-2,3,7,13,17,18-hexamethyl-1,10,19,21,23,24-hexahydro-1,19-dioxobilin (2). 3-Nor-neoxanthobilirubic acid (**7**) 548 mg, 2.00 mmole) was placed into a 25 mL round bottom flask along with a small magnetic stir bar. The flask was then fitted with a rubber septum and 10 mL of dichloromethane was added. After flushing the system with N_2 for several minutes, 1-formyladamantane³⁰ (171 mg, 2.20 mmole) and TFA (500 μL) were added via a syringe. Upon addition of the acid, the mixture became homogeneous and reddish orange. It was allowed stir under N_2 at room temperature for 5 hrs; then the dark solution was taken up in 100 mL of dichloromethane and washed with water and saturated aq. NaCl. After drying over anhydr. Na_2SO_4 , the solution was evaporated to give a dark solid, which was initially purified by flash-column chromatography on silica gel eluting with dichloromethane-methanol 100:2 (by vol). The resulting orange solid was further purified by radial chromatography, eluting with dichloromethane-methanol 100:2

(by vol) to afford 430 mg (31%) of the desired bright yellow pigment (**2**). It had mp 280°C (dec); IR (KBr) ν : 3416, 2908, 1692, 1683, 1648, 1492, 1438, 1259, 1216, 1173, 1055 cm^{-1} ; and $^1\text{H-NMR}$ and $^{13}\text{C-NMR}$ spectral data in Tables 1 and 2. An analytical sample was prepared by dissolving the sample in a minimum amount of hot CH_2Cl_2 and precipitating it out by the addition of hexane. The bright yellow pigment was filtered and dried over P_2O_5 overnight.

<i>Anal.</i> Calcd. for $\text{C}_{41}\text{H}_{50}\text{N}_4\text{O}_6$ (694.9):	C, 70.87; H, 7.25; N, 8.06.
Calcd. for $\text{C}_{41}\text{H}_{50}\text{N}_4\text{O}_6 \cdot 1/2 \text{H}_2\text{O}$ (703.9):	C, 69.96; H, 7.16; N, 7.96.
Found:	C, 69.80; H, 7.13; N, 7.72.

10-(1-Adamantyl)-8,12-bis-(2-methoxycarbonylethyl)-2,3,7,13,17,18-hexamethyl-1,10,19,21,23,24-hexahydro-1,19-dioxobilin (4). Cesium carbonate (130 mg, 0.674 mmole) followed by iodomethane (26.0 μL , 0.405 mmole) was added to a solution of (**2**) (120 mg, 0.174 mmole) in dry DMF (3.50 mL) and stirred at room temperature for 4 hrs. Additional iodomethane was added (26.0 μL) and the solution was allowed to continue to stir overnight. The yellow solution was then taken up in 50 mL of dichloromethane and extracted with water (3×100 mL), dried over anhydr. Na_2SO_4 , and evaporated to give an oil still containing some DMF. The oil was placed under high vacuum for a day, and the solid residue was purified by radial chromatography. Elution with dichloromethane-methanol 100:3 (by vol) afforded 103 mg of the desired diester (**4**) as a bright yellow solid (81.7%). It had mp 280°C (dec). IR (KBr) ν : 3380, 2906, 2849, 1739, 1680, 1630, 1436, 1348, 1262, 1167, 1054, 1015 cm^{-1} ; and $^1\text{H-NMR}$ and $^{13}\text{C-NMR}$ reported in Tables 3 and 2. An analytical sample was prepared by the addition of hexane to a dichloromethane solution of the pigment followed by slow evaporation of the solvents under a stream of nitrogen. The resultant bright yellow crystals were collected by filtration and dried over P_2O_5 in a drying pistol overnight.

<i>Anal.</i> Calcd. for $\text{C}_{43}\text{H}_{54}\text{N}_4\text{O}_6$ (722.9):	C, 71.44; H, 7.53; N, 7.75.
Found:	C, 72.01; H, 7.59; N, 7.42.

10-tert-Butyl-8,12-bis-(2-carboxyethyl)-2,3,7,13,17,18-hexamethyl-1,10,19,21,23,24-hexahydro-1,19-dioxobilin bis-amide with S-(+)-alanine methyl ester (8). C(10)-tert-Butyl rubin **1** (61.6 mg, 0.1 mmole), S-(+)-alanine methyl ester hydrochloride (140 mg, 1 mmole), diphenylphosphoryl azide (112 mg, 1 mmole, 88 μL), and triethylamine (204 mg, 2 mmole, 282 μL) were mixed in 2 mL of dry DMSO at room temperature and stirred in the dark for 20 hours. To the clear, slightly green solution was added 80 mL of CH_2Cl_2 , and the solution was washed with water (3×40 mL). During the work-up the color became bright yellow once again. The organic layer was dried over anhydr. Na_2SO_4 and evaporated to afford a yellow film, which was purified by radial chromatography (eluting with 100:4 (by vol.) CH_2Cl_2 :MeOH) to give 55.2 mg (70%) of the desired bright yellow bis-amide after crystallization from CH_2Cl_2 -MeOH-*n*-hexane. It had mp 170°C (dec); IR (KBr) 3423, 3292, 2954, 2856, 1742, 1671, 1656, 1649, 1639, 1540, 1440, 1352, 1252, 1207, 1164, 1058, 942 cm^{-1} ; $^1\text{H-NMR}$ (CDCl_3) δ : 1.12 (s, 9H), 1.44 (d, 3H, J=7 Hz), 1.48 (d, 3H, J=7 Hz), 1.58 (s, 6H), 2.17 (s, 12H), 2.38 (m, 4H), 2.87 (m, 4H), 3.75 (s, 6H), 4.22 (s, 1H), 4.60 (q, 2H, J=7 Hz), 5.87 (brs, 1H), 5.77 (brs, 1H), 6.90 (brs, 1H, CONH), 7.32 (brs, 1H, CONH), 8-9 ppm (vbrs, 2H, NH), 9.63 (brs, 1H, NH), 9.78 (brs, 1H, NH) ppm. $^1\text{H-NMR}$ ($(\text{CD}_3)_2\text{SO}$) δ : 0.98 (s, 9H), 1.21 (d, 3H, J=7 Hz), 1.25 (d, 3H, J=7 Hz), 1.74 (s, 6H), 1.95 (s, 6H), 2.03 (s, 6H), 2.13 (m, 4H), 2.57 (m, 4H), 3.58 (s, 3H), 3.59 (s, 3H), 4.0 (s, 1H), 4.23 (q, 2H, J=7 Hz), 5.98 (s, 2H), 8.18 (d, 1H, J=7 Hz, CONH), 8.23 (d, 1H, J=7 Hz, CONH), 9.34 (s, 1H, NH), 9.37 (s, 1H, NH), 9.67 (s, 2H, NH) ppm.

<i>Anal.</i> Calcd. for $\text{C}_{43}\text{H}_{58}\text{N}_6\text{O}_8$ (786.9):	C, 65.06; H, 7.53; N, 10.46.
Found:	C, 65.21; H, 7.30; N, 10.02.

10-(1-Adamantyl)-8,12-bis-(2-carboxyethyl)-2,3,7,13,17,18-hexamethyl-1,10,19,21,23,24-hexahydro-1,19-dioxobilin bis-amide with S-(+)-alanine methyl ester (9). C(10)-Adamantyl rubin (**2**) (69.5 mg, 0.1 mmole) was converted as above for **8** to 65.2 mg (75%) of the bis-amide (**9**) with S-(+)-alanine methyl ester. It had mp 200°C (dec); IR (KBr) ν : 3425, 2907, 2840, 1742, 1692, 1641, 1451, 1382, 1263, 1217, 1110, 1060 cm^{-1} ; $^1\text{H-NMR}$

NMR ((CD₃)₂SO) δ : 1.22 (d, 3H, J=7 Hz), 1.25 (d, 3H, J=7 Hz), 1.56 (brs, 12H, adamantane α and γ H's), 1.74 (s, 6H), 1.92 (s, 3H, adamantane β H's), 1.96 (s, 6H), 2.03 (s, 6H), 2.14 (m, 4H), 2.59 (m, 4H), 3.587 (s, 3H, OCH₃), 3.593 (s, 3H, OCH₃), 3.88 (s, 1H), 4.239 (q, 1H, J=7 Hz), 4.235 (q, 1H, J=7 Hz), 5.98 (s, 2H), 8.22 (d, 1H, J=7 Hz, CONH), 8.27 (d, 1H, J=7 Hz, CONH), 9.36 (s, 1H, NH), 9.39 (s, 1H, NH), 9.70 (s, 2H, NH) ppm.

<i>Anal.</i> Calcd. for C ₄₉ H ₆₄ N ₆ O ₈ (865.1):	C, 68.03; H, 7.46; N, 9.71.
Calcd. for C ₄₉ H ₆₄ N ₆ O ₈ · 1/2 CH ₃ OH (881.1):	C, 67.47; H, 7.55; N, 9.54.
Found:	C, 67.30; H, 7.40; N, 9.41.

Molecular Dynamics. Molecular mechanics calculations and molecular modelling were carried out on an Evans and Sutherland ESV-10 workstation using version 6.0 of SYBYL (Tripos Assoc., St. Louis, MO). The dipyrinone units of **1** and **2** were rotated independently about the central CHR at C(10) (torsion angles ϕ_1 and ϕ_2) through 10° increments from 0° to 360°. (The $\phi_1=0^\circ$, $\phi_2=0^\circ$ conformer has a porphyrin shape.) In this procedure the two torsion angles were held fixed at each increment while the remainder of the molecule was relaxed to its minimum energy conformation using molecular mechanics. This was followed by a molecular dynamics cooling curve consisting of the following temperatures and times: 100 fs at 20°K, 100 fs at 10°K, 100 fs at 5°K, 200 fs at 2°K, 200 fs at 1°K, 200 fs at 0.5°K, 300 fs at 0.1°K. This was followed by molecular mechanics minimization, which gave the lowest energy conformations for each set of ϕ values. The conformational energy maps were created using Wingz™ (Informix), and the ball and stick drawings were created from the atomic coordinates of the molecular dynamics structures using Müller and Falk's "Ball and Stick" program (Cherwell Scientific, Oxford, U.K.) for the Macintosh.

Acknowledgments: We thank the National Institutes of Health (HD17779) for generous support. Ari Kar acknowledges receipt of a Wilson Graduate Fellowship.

References

1. Dhowdury, J.R.; Wolkoff, A.W.; Chowdury, N.R.; Arias, I.M. Hereditary Jaundice and Disorders of Bilirubin Metabolism. In *The Metabolic and Molecular Bases of Inherited Disease* (Scriver, C.R., Beaudet, A.L., Sly, W.S., Valle, D., eds.) McGraw-Hill Inc., New York, 1979, Vol. II, 2161-2208.
2. Falk, H. *The Chemistry of Linear Oligopyrroles and Bile Pigments*, Springer Verlag, Wien, 1989.
3. McDonagh, A.F. In *The Porphyrins*; Dolphin, D., ed., Academic Press, New York, 1979; Vol. 6, pp 293-491.
4. Person, R.V.; Peterson, B.R.; Lightner, D.A. *J. Am. Chem. Soc.* **1994**, *116*, 42-59.
5. (a) Bonnett, R.; Davies, J.E.; Hursthouse, M.B.; Sheldrick, G.M. *Proc. R. Soc. London, Ser. B* **1978**, *202*, 249-268.
(b) LeBas, G.; Allegret, A.; Mauguén, Y.; DeRango, C.; Bailly, M. *Acta Crystallogr., Sect. B* **1980**, *B36*, 3007-3011.
(c) Becker, W.; Sheldrick, W.S. *Acta Crystallogr., Sect. B* **1978**, *B34*, 1298-1304.
6. (a) Kaplan, D.; Navon, G. *Israel J. Chem.* **1983**, *23*, 177-186.
(b) Kaplan, D.; Navon, G. *Org. Magn. Res.* **1983**, 198.
(c) Kaplan, D.; Navon, G. *Biochem. J.* **1982**, *201*, 605-613.
(d) Navon, G.; Frank, S.; Kaplan, D. *J. Chem. Soc. Perkin Trans. 2* **1984**, 1145-1149.
7. McDonagh, A.F.; Lightner, D.A. In *Hepatic Metabolism and Disposition of Endo and Xenobiotics* (Falk Symposium No. 57, Bock, K.W.; Gerok, W.; Matern, S., eds.) Kluwer, Dordrecht, The Netherlands, **1991**, Chap. 5, pp 47-59.
8. Blanckaert, N.; Heirwegh, K.P.M.; Zaman, Z. *Biochem. J.* **1977**, *164*, 229-236.

9. Manitto, P.; Monti, D. *J.C.S. Chem. Commun.* **1976**, 122-123.
10. (a) Xie, M.; Lightner, D.A. *Tetrahedron* **1993**, *49*, 2185-2200.
(b) Xie, M.; Holmes, D.L.; Lightner, D.A. *Tetrahedron* **1993**, *49*, 9235-9250.
11. Falk, H.; Müller, N.; Wöss, H. *Monatsh. Chem.* **1989**, *120*, 35-43.
12. Kar, A.; Lightner, D.A. *Tetrahedron* **1998**, in press.
13. Shioiri, T.; Hinomiya, K.; Yamada, S. *J. Am. Chem. Soc.* **1972**, *94*, 6203-6205.
14. Nogales, D.F.; Ma, J-S.; Lightner, D.A. *Tetrahedron* **1993**, *49*, 2361-2372.
15. Boiadjiev, S.E.; Anstine, D.T.; Lightner, D.A. *J. Am. Chem. Soc.* **1995**, *117*, 8727-8736.
16. (a) Trull, F.R.; Ma, J.S.; Landen, G.L.; Lightner, D.A. *Israel J. Chem.* **1983**, *23*, 211-218.
(b) Lightner, D.A.; Trull, F.R. *Spectrosc. Lett.* **1983**, *16*, 785-803.
(c) Lightner, D.A.; Ma, J-S. *Spectrosc. Lett.* **1984**, *17*, 317-327.
17. Boiadjiev, S.E.; Lightner, D.A. *Tetrahedron: Asymmetry* **1997**, *8*, 2115-2129.
18. (a) Gawroński, J.K.; Połonski, T.; Lightner, D.A. *Tetrahedron* **1990**, *46*, 8053-8066.
(b) Trull, F.R.; Shrout, D.P.; Lightner, D.A. *Tetrahedron* **1992**, *48*, 8189-8198.
19. (a) Lightner, D.A.; Ma, J-S.; Adams, T.C.; Franklin, R.W.; Landen, G.L. *J. Heterocyclic Chem.* **1984**, *21*, 139-144.
(b) Trull, F.R.; Franklin, R.W.; Lightner, D.A. *J. Heterocyclic Chem.* **1987**, *24*, 1573-1579.
(c) Puzicha, G.; Pu, Y-M.; Lightner, D.A. *J. Am. Chem. Soc.* **1991**, *113*, 3583-3592.
20. Boiadjiev, S.E.; Pfeiffer, W.P.; Lightner, D.A. *Tetrahedron* **1997**, *53*, 14547-14564.
21. Shrout, D.P.; Puzicha, G.; Lightner, D.A. *Synthesis* **1992**, 328-332.
22. (a) Lightner, D.A.; Gawroński, J.; Wijekoon, W.M.D. *J. Am. Chem. Soc.* **1987**, *109*, 6354-6362.
(b) Lightner, D.A.; Reisinger, M.; Wijekoon, W.M.D. *J. Org. Chem.* **1987**, *52*, 5391-5395.
(c) Lightner, D.A.; Person, R.V.; Peterson, B.R.; Puzicha, G.; Pu, Y-M.; Bojadziev, S. *Biomolecular Spectroscopy II* (Birge, R.R.; Nafie, L.A., eds.), Proc. SPIE 1432, **1991**, 2-13.
23. (a) Harada, N.; Nakanishi, K. *Circular Dichroic Spectroscopy - Exciton Coupling in Organic Stereochemistry*, University Science Books, Mill Valley, CA, 1983.
(b) Kasha, M.; Rawls, H.R.; El-Bayoumi, M.A. *Pure Appl. Chem.* **1965**, *32*, 371-392.
24. Falk, H.; Schlederer, T.; Wohlschann, P. *Monatsh. Chem.* **1981**, *112*, 199-207.
25. Barnes, J.C.; Paton, J.D.; Damewood, J.R. Jr., Mislow, K. *J. Org. Chem.* **1981**, *46*, 4975-4979.
26. (a) Falk, H.; Müller, N. *Monatsh. Chem.* **1982**, *112*, 1325-1332.
(b) Falk, H.; Müller, N. *Tetrahedron* **1983**, *39*, 1875-1885.
27. (a) Bonnett, R.; Davies, J.E.; Hursthouse, M.B.; Sheldrick, G.M. *Proc. R. Soc. London, Ser. B* **1978**, *202*, 249-268.
(b) LaBas, G.; Allegret, A.; Mauguen, Y.; DeRango, C.; Bailly, M. *Acta Crystallogr., Sect. B* **1980**, *B36*, 3007-3011.
28. Lightner, D.A.; Wijekoon, W.M.D.; Zhang, M-H. *J. Biol. Chem.* **1988**, *263*, 16669-16676.
29. Puzicha, G.; Pu, Y-M.; Lightner, D.A. *J. Am. Chem. Soc.* **1991**, *113*, 3583-3592.
30. Stetter, H.; Rauscher, E. *Chem. Ber.* **1960**, *93*, 1161-1166.